Template-Based Preparation of Free-Standing Semiconducting Polymeric Nanorod Arrays on Conductive Substrates

Niko Haberkorn,[†,‡] Stefan A. L. Weber,[‡] Rüdiger Berger,[‡] and Patrick Theato*[,†,§]

Institute of Organic Chemistry, University of Mainz, Duesbergweg 10-14, 55099 Mainz, Germany, Max Planck Institute for Polymer Research, Ackermannweg 10, 55128 Mainz, Germany, and School of Chemical and Biological Engineering, WCU Program of Chemical Convergence for Energy & Environment (C2E2), College of Engineering, Seoul National University, 151-744 Seoul, Korea

ABSTRACT We describe the synthesis and characterization of a cross-linkable siloxane-derivatized tetraphenylbenzidine (DTMS-TPD), which was used for the fabrication of semiconducting highly ordered nanorod arrays on conductive indium tin oxide or Pt-coated substrates. The stepwise process allow fabricating of macroscopic areas of well-ordered free-standing nanorod arrays, which feature a high resistance against organic solvents, semiconducting properties and a good adhesion to the substrate. Thin films of the TPD derivate with good hole-conducting properties could be prepared by cross-linking and covalently attaching to hydroxylated substrates utilizing an initiator-free thermal curing at 160 °C. The nanorod arrays composed of cross-linked DTMS-TPD were fabricated by an anodic aluminum oxide (AAO) template approach. Furthermore, the nanorod arrays were investigated by a recently introduced method allowing to probe local conductivity on fragile structures. It revealed that more than 98% of the nanorods exhibit electrical conductance and consequently feature a good electrical contact to the substrate. The prepared nanorod arrays have the potential to find application in the fabrication of multilayered device architectures for building well-ordered bulk-heterojunction solar cells.

KEYWORDS: nanorod arrays • anodic aluminum oxide (AAO) • tetraphenylbenzidine • organic photovoltaics • conductive scanning force microscopy

INTRODUCTION

In recent years, there has been a remarkable progress in patterning of conducting organic and polymeric materials for electronic and optoelectronic applications (1, 2). Besides commonly used techniques like photolithography (3, 4) and inkjet printing (5, 6), the use of nanoporous templates has gained increasing attention for nanoscopic patterning of inorganic (7–10) as well as organic materials. As such, nanoporous templates have proven to be a versatile tool for the fabrication of well-ordered arrays of nanorods and tubes (11).

In particular, it has been widely proposed that such nanorod arrays composed of semiconducting materials, which are attached to a conductive substrate and can subsequently be embedded into a semiconducting matrix, are the ideal morphological architecture for organic solar cell devices with high performances (12–14). Such morphologies would provide not only a nanoscopic interpenetrating donor/acceptor network with an interfacial distance in the range of the exciton diffusion length (approximately 10−20 nm) but also percolated pathways to guarantee charge transport to the electrodes.

Nanoporous templates, e.g., anodic aluminum oxide (AAO) membranes (15–19) and block copolymer templates (20–22), provide uniform and well-ordered nanopores with large lateral pore densities up to 1×10^{11} cm^{-2} (23, 24). The templates can be filled with the semiconducting materials by electrodeposition (25), electropolymerization (26–28) or by wetting of polymer melts or solutions (in the case of AAO) (29–31). Accordingly, arrays of nanorods composed of several conducting and semiconducting polymers have been fabricated by applying such a template-assisted approach (32–36). However, one of the crucial issues especially for polymeric nanorods is to prevent the rods from collapsing and aggregating after selective removal of the template (37). Furthermore, the patterned semiconducting material should provide a good adhesion to the conductive substrate and a good chemical resistance against organic solvents in order to enable subsequent spin-coating steps, which are required for a solution-based preparation of organic photovoltaic cells.

In this paper, we present the fabrication of large arrays of free-standing nanorods composed of a cross-linked siloxane-derivatized tetraphenylbenzidine (TPD) on conductive substrates by applying an AAO-assisted templating technique, following a procedure that had been published recently (38). Siloxane-derivatized TPDs, first pioneered by Marks and co-workers as self-assembled hole-injecting layers on ITO surfaces to improve the device performance of organic light emitting diodes (39–43), were used as a class

* To whom correspondence should be addressed. e-mail: theato@uni-mainz.de; phone: +49-6131-3926256; fax: +49-6131-3924778.
Received for review February 1, 2010 and accepted April 16, 2010
† University of Mainz.
‡ Max Planck Institute for Polymer Research.
§ Seoul National University.
DOI: 10.1021/am100085t
2010 American Chemical Society

of hole-conducting TPDs, which is also highly suitable for the fabrication of nanorod arrays on conducting substrates because it provides both the hole-conducting properties of the TPD mojeties and the organosilanol groups that can covalently bind to a substrate and cross-link. As a consequence, delamination of the nanorod arrays during the fabrication can be drastically decreased and large areas of free-standing nanorods can be obtained, which show a high resistance against organic solvents.

EXPERIMENTAL SECTION

Instrumentation. All ^{1}H and ^{13}C NMR spectra were recorded on a Bruker 300 MHz FT-NMR spectrometer. ^{29}Si-MAS NMR spectra were measured on a Bruker DSX 400 MHz FT NMR spectrometer (rotation: 5000 Hz, 4 mm rotor). Chemical shifts (δ) were given in parts per million (ppm) relative to TMS. Thermogravimetric analysis (TGA) was performed using a Perkin-Elmer Pyris 6 TGA in nitrogen atmosphere (10 mg of the compound in an aluminum pan). Cyclovoltametric measurements were performed using an Autolab PGSTAT30 (Eco Chemie) Potentiosat/Galvanostat. Pt wire and Ag/AgCl were used as the counter and reference electrode, respectively. The hole-conducting polymer film on ITO/glass was used as the working electrode and 0.1 M tetrabutylammonium tetrafluoroborate ($TBABF_4$) in acetonitrile was used as electrolyte. HOMO values were determined relative to ferrocene.

SEM images were recorded using a Zeiss Leo 1530 at an acceleration voltage of 3.0 kV for AAO membranes and 0.7 kV for polymeric samples. For detection, an Inlens detector was used. Conductive scanning torsion mode microscopy (SCTMM) measurements were performed with a Veeco MultiMode (NanoScope IIIa Controller with Quadrex-extender and current amplifier TUNA, sensitivity 1 pA/V) using rectangular PtIr-coated cantilevers (Nanosensors PPP-EFM, Switzerland) with a vertical and a torsional resonance frequency of 50 − 80 kHz and 700 − 900 kHz, respectively. The typical amplitude of the lateral tip movement at resonance was in the range of 2−5 nm. All experiments were performed at ambient conditions (21 °C, relative humidity 30−50%).

Materials. All reagents were purchased from Aldrich, Fluka and Acros and were used without further purification unless otherwise stated. Toluene and tetrahydrofuran (THF) were distilled from sodium/potassium. The syntheses were carried out under argon atmosphere using standard Schlenk techniques. ITO-coated glass substrates with sheet resistance of <10 Ohm/sq were purchased from Präzisions Glas & Optik GmbH, Germany, and were cleaned by ultrasonication in aqueous Helmanex (1 wt %), isopropyl alcohol, and acetone. Prior measurements, they were dried with a stream of pressurized N_2 and subjected to O_2 plasma cleaning for 10 min.

Synthesis. ***General Procedure for Buchwald−Hartwig Arylation.*** Tris(dibenzylideneacetone)dipalladium(0) (Pd_2dba_3) (2 mol % according to the amine reagent) and 1,1′-bis(diphenylphosphino)ferrocene (DPPF) (4 mol % according to the amine reagent) were dissolved in toluene under argon and degassed by two freeze−pump−thaw cycles. This activated catalyst was then added to a degassed mixture of the bromoaryl compound (1.0 eq of bromo units), the aromatic amine (1.0 equiv) and sodium-*tert*-butylate (2.8 equiv) in toluene. The mixture was stirred for 15 h at 90 °C. After the mixture was cooled to room temperature, the reaction was quenched by adding 5 mL of methanol, diluted with diethylether, and washed twice with brine and water, respectively. The combined aqueous phase was extracted twice with diethylether. The combined organic phase was then dried with $MgSO_4$, filtered, and the solvent evaporated under reduced pressure. The residue was purified by column chromatography on silica gel with petrol ether/ethyl acetate (9:1 v/v).

Synthesis of N-(4-Methoxyphenyl)-N-phenyl-amine (1). *N*-(4-Methoxy-phenyl)-*N*-phenyl-amine was synthesized according to the general procedure for Buchwald−Hartwig arylation described above starting from 4-bromoanisol and aniline (yield 86%).

^{1}H NMR (300 MHz, $CDCl_3$): δ 3.79 (s, 3H, −OMe), 5.50 (s, br, 1H, NH), 6.80−6.91 (m, 4H, Ar−H), 7.02 −7.12 (m, 2H, Ar−H), 7.21 (t, 2H, $^{3}J_{H-H}$ = 8.5 Hz, Ar−H).

^{13}C NMR (75 MHz, $CDCl_3$): δ/ppm= 55.6, 114.7, 115.7, 119.6, 122.2, 129.3.

Synthesis of N,N2-Bis(4-methoxyphenyl)-N,N2-bisphenyl-1,12-bisphenyl-4,42-diamine (2). *N,N′*-Bis(4-methoxyphenyl)-*N,N*-bisphenyl-1,1′-bisphenyl-4,4′-diamine was synthesized according to the general procedure for Buchwald−Hartwig arylation described above starting from *N*-(4-methoxyphenyl)-*N*-phenyl-amine and 4,4′-dibromodiphenyl (yield 92%).

^{1}H NMR (300 MHz, $CDCl_3$): δ/ppm 3.80 (s, 6H, −OMe), 6.85 (d, 4H, $^{3}J_{H-H}$ = 8.7 Hz, Ar−H), 6.96 (t, 2H, $^{3}J_{H-H}$ = 8.5 Hz, Ar−H_{para}), 7.04−7.13 (m, 12H, Ar−H), 7.22 (t, 4H, $^{3}J_{H-H}$ = 8.5 Hz, Ar−H), 7.40 (d, 4H, $^{3}J_{H-H}$ = 8.5 Hz, Ar−H).

Synthesis of N,N2-Bis(4-methoxyphenyl)-N,N2-bis(4-formylphenyl)-(1,12-biphenyl)-4,42-diamine (3). Ten grams (18.23 mmol) of **2** was dissolved in 120 mL of dry *N*,*N*-dimethylformamide. The solution was cooled down to 0 °C and 24.95 mL (273.0 mmol, 15.0 equiv) of phosphoroxychloride were added dropwise. The mixture was stirred at 90 °C for 15 h. After cooling to room temperature the mixture was poured on 500 g of ice and neutralized with 5 N sodium hydroxide solution. The precipitate was filtered off, washed with water and dried at 50 °C in vacuo. The crude product was purified by flash column chromatography (silica gel, petrol ether/ethyl acetate 9:1) to yield 6.64 g (11.0 mmol, 60% yield) of **3** as a yellow crystalline powder.

^{1}H NMR (300 MHz, $CDCl_3$): δ/ppm 3.81 (s, 6H, −OMe), 6.90 (d, 4H, $^{3}J_{H-H}$ = 8.5 Hz, Ar−H), 6.99 (d, 2H, $^{3}J_{H-H}$ = 8.5 Hz, Ar−H), 7.13 (d, 4H, Ar−H), 7.20 (d, 4H, $^{3}J_{H-H}$ = 8.5 Hz, Ar−H), 7.49 (d, 4H, $^{3}J_{H-H}$ = 8.5 Hz, Ar−H), 7.66 (d, 4H, $^{3}J_{H-H}$ = 8.5 Hz, Ar−H), 9.77 (s, 2H, Ar−C(=O)H).

^{13}C NMR (75 MHz, $CDCl_3$): δ/ppm 55.5, 115.2, 118.6, 125.7, 127.9, 128.5, 128.7, 131.4, 136.4, 136.7, 145.4, 153.4, 157.6, 190.4.

Synthesis of N,N2-Bis(4-methoxyphenyl)-N,N2-bis(4-(hydroxymethyl)-phenyl)- (1,12-biphenyl)-4,42-diamine (4). **3** (6.64 g, 11.0 mmol) was dissolved in a mixture of 150 mL of dry ethanol and 60 mL of dry dichloromethane. Sodium borohydride (3.20 g, 84.6 mmol) was added stepwise and the mixture was stirred for 20 h at room temperature. The reaction was quenched by slowly adding water. The solvent was then evaporated; the residue was redissolved in 150 mL of dichloromethane and washed twice with brine and water, respectively. The combined aqueous phases were extracted with dichloromethane and the organic phases were then dried over magnesium sulfate and the solvent was evaporated in vacuo. Purification of the residue by flash column chromatography (silica gel, petrol ether/ethyl acetate 1:4) yielded 6.40 g (10.5 mmol, 96% yield) of **4** as a green crystalline powder.

^{1}H NMR (300 MHz, $CDCl_3$): δ/ppm 3.79 (s, 6H, -OMe), 4.59 (s, 4H, Ar−CH_2−OH), 6.84 (d, 4H, $^{3}J_{H-H}$ = 8.5 Hz, Ar−H), 7.01−7.10 (m, 12H, Ar−H), 7.21 (d, 4H, $^{3}J_{H-H}$ = 8.5 Hz, Ar−H), 7.38 (d, 4H, $^{3}J_{H-H}$ = 8.8 Hz, Ar−H).

^{13}C NMR (75 MHz, $CDCl_3$): δ/ppm= 55.5, 65.1, 114.8, 122.9, 127.2, 127.3, 128.3, 129.1, 131.7, 134.0, 134.1, 134.2, 134.3, 146.9, 147.6, 156.3.

Synthesis of N,N2-Bis(4-methoxyphenyl)-N,N2-bis(4-(allyloxymethyl)-phenyl)-(1,12-biphenyl)-4,42-diamine (5). Three grams (4.93 mmol) of **4** was dissolved in 100 mL of dry tetrahydrofuran, cooled to 0 °C, and 0.75 g (31.25 mmol) of

sodium hydride were added in small portions. After stirring for 1 h at room temperature, 1.79 g (14.8 mmol) of allyl bromide were added dropwise at 0 °C and the mixture was stirred at 50 °C for 5 h. Residues of sodium hydride were removed by slowly adding water. The solvent was then evaporated in vacuo, the residue was dissolved in diethyl ether and washed with brine and water twice. The organic phase was dried over magnesium sulfate and the solvent was removed under reduced pressure. The residue was purified by flash column chromatography on silica gel (petrol ether/ethyl acetate 4:1) to yield 2.30 g (3.34 mmol, 68% yield) of **5** as a slightly yellow solid.

^{1}H NMR (300 MHz, $CDCl_3$): δ/ppm 3.79 (s, 6H, −OMe), 4.04 (d, 4H, $^3J_{H-H}$ = 5.6 Hz, O−C$\underline{H}_2$−CH=CH_2), 4.44 (s, 4H, Ar−C$\underline{H}_2$−O), 5.20 (dd, 2H, $^3J_{H-H}$ = 10.3 Hz, $^2J_{H-H}$ = 1.5 Hz, O−CH_2−CH=$CH_{cis}\underline{H}_{trans}$), 5.31 (dd, 2H, $^3J_{H-H}$ = 17.2 Hz, $^2J_{H-H}$ = 1.5 Hz, O−CH_2−CH=C$\underline{H}_{cis}H_{trans}$), 5.96 (ddd, 2H, $^3J_{H-H}$ = 17.2 Hz, $^3J_{H-H}$= 10.3 Hz, $^3J_{H-H}$ = 5.5 Hz, O−CH_2−C$\underline{H}$=$CH_{cis}H_{trans}$), 6.84 (d, 4H, $^3J_{H-H}$ = 8.7 Hz, Ar−$\underline{H}$), 7.03 (d, 4H, $^3J_{H-H}$ = 8.5 Hz, Ar−$\underline{H}$), 7.05 (d, 4H, $^3J_{H-H}$ = 8.7 Hz, Ar−$\underline{H}$), 7.08 (d, 4H, $^3J_{H-H}$ = 8.8 Hz, Ar−$\underline{H}$), 7.20 (d, 4H, $^3J_{H-H}$ = 8.5 Hz, Ar−$\underline{H}$), 7.39 (d, 4H, $^3J_{H-H}$ = 8.8 Hz, Ar−$\underline{H}$).

Synthesis of N,N2-Bis(4-methoxyphenyl)-N,N2-bis(4-((3-(trimethoxysilyl)propoxy) methyl)-phenyl)-(1,12-biphenyl)-4,42-diamine (DTMS-TPD). With the use of standard Schlenk technique, 20 mg of platinum on carbon (5 wt % loading) was added to a solution of 5 (2.3 g, 3.34 mmol) in dry toluene (50 mL). One and a half milliliters (11.78 mmol) of trimethoxysilane was added dropwise at room temperature and the mixture was heated to 90 °C for 24 h. After being cooled to room temperature, the mixture was filtrated twice over Celite under inert atmosphere to remove the catalyst. The solvent was evaporated under reduced pressure and the residue was purified by column chromatography on silica gel (chloroform, under inert atmosphere). **6** (1.62 g, 1.73 mmol, 52%) was obtained as a yellow viscous oil and stored at −20 °C under an inert atmosphere.

^{1}H NMR (300 MHz, $CDCl_3$): δ/ppm 0.70 (m, 4H, −CH_2−Si$(OMe)_3$), 1.66−1.78 (m, 4H, O−CH_2−C$\underline{H}_2$), 3.46 (t, 4H, $^3J_{H-H}$ = 7.0 Hz, O−C$\underline{H}_2$−CH_2), 3.55 (s, Si$(OCH_3)_3$), 3.79 (s, 6H, −OMe), 4.41 (s, 4H, Ar−C$\underline{H}_2$−O), 6.83 (d, 4H, $^3J_{H-H}$ = 8.7 Hz, Ar−$\underline{H}$), 7.00−7.11 (m, 12H, Ar−$\underline{H}$), 7.18 (d, 4H, $^3J_{H-H}$ = 8.5 Hz, Ar−$\underline{H}$), 7.38 (d, 4H, $^3J_{H-H}$ = 8.8 Hz, Ar−$\underline{H}$). FD mass spectra (*m*/*z*): 931.8 (calcd mass: 932.4 g/mol).

Preparation of Nanorod Arrays. A thin AAO template that was fabricated by a two-step anodization process and still mechanically stabilized on the remaining aluminum layer was spin-coated with a diluted, precondensed DTMS-TPD solution (6 wt % in toluene, 60 min stirring at atmospheric conditions before coating, 2000 rpm). The complete coated templates were then dried in vacuo and cut into several parts with a razor blade to prepare several samples. The cleaned substrates, like ITO/glass, Pt-coated silicon, and quartz, were pressed on the coated template and clamped together. Air inclusions between substrate and TPD films were removed by vacuum treatment. A PDMS layer between the aluminum and the pressing plate was used to homogenize the imprinting pressure all over the sample. The samples were heated to 50 °C for 1 h and then thermally cross-linked at 160 °C for 4 h. The aluminum and the AAO were selectively etched away by treatment with aqueous $CuCl_2$ (c = 0.2 mol L^{-1}) and aqueous phosphoric acid (10 wt %, 90 min). After repeated rinsing and dipping cycles with deionized water, the samples were dried by freeze-drying.

RESULTS AND DISCUSSION

Following the concept of well organized interpenetrating phases of organic hole- and electron-conductors that might find application for all-organic based photovoltaics, we recently reported on the thermal cross-linking of divinyltriphenylamine, which was used to fabricate successfully free-standing nanorod arrays. However, in order to obtain a suitable adhesion and covalent binding of triphenylamine derivatives on ITO/glass, the substrate had to be prefunctionalized with an organosiloxane. But still the templating of large areas remained a delicate issue due to partial delamination. To abandon the prefunctionalization step of the substrate and to optimize the large-area patterning process avoiding delamination, we designed a siloxane-derivatized TPD.

Synthesis. The bifunctional organosiloxane-derivatized tetraphenylbenzide *N*,*N*2-bis(4-methoxyphenyl)-*N*,*N*2-bis(4-((3-(trimethoxysilyl)propoxy)methyl)-phenyl)-(1,12biphenyl)4,42-diamine (DTMS-TPD) was synthesized in a six-step reaction (see Scheme 1A). TPD-based materials are known to be suitable hole conductors and the trimethoxysilane groups allow for covalently binding to hydroxyl functionalities of an ITO surface and for formation of cross-linked siloxane-based networks by thermally induced condensation.

In a sequential palladium-catalyzed Buchwald−Hartwig arylation, aniline was allowed to react with *p*-bromoanisole to afford the secondary amine **1**, which was then coupled with 4,4′-dibromodiphenyl to yield the dimethoxy substituted TPD **2**. In a double Vilsmeyer−Haack formylation using phosphoroxychloride and *N*,*N*-dimethylformamine compound **3** was obtained, which was subsequently converted to the dimethylenehydroxy substituted TPD **4** by reduction with sodium borohydride in quantitative yields. Etherfication with allyl bromide using sodium hydride as a base, afforded the tethered divinyl substituted TPD **5**. Compound **5** was coupled with trimethoxysilane to yield the corresponding disiloxane derivatized TPD (DTMS-TPD) via platinum catalyzed hydrosilylation. The compound DTMS-TPD was successfully identified and characterized by NMR and mass spectroscopy.

Characterization and Thin Film Preparation. The thermogravimetric analysis (TGA) (see the Supporting Information, Figure S2) of DTMS-TPD showed a slight weight loss (approximately 7%) starting at 100 °C, which indicates the thermally induced condensation of the two trimethoxysilane groups (see Scheme 1B). The thermal-induced decomposition of the cross-linked material started above 250 °C and therefore the compound provides a suitable thermal stability for the cross-linking step. To study the cross-linking characteristics in more detail, we performed solid state ^{29}Si-MAS NMR spectroscopy. The ^{29}Si chemical shift values of the organosiloxane units allowed to clearly distinguish between T_0, T_1, T_2, and T_3 branches, which indicate the degree of self-condensation (44, 45). The T_0 corresponds to the noncondensed R-Si$(OMe)_3$ unit and the T_3 branch indicates the fully condensed R-Si$(OSi\text{-}R)_3$ unit (T_x: R-Si$(OSi)_x(OMe)_{3-x}$).

Before thermal treatment of DTMS-TPD, the ^{29}Si-MAS NMR spectrum showed signals at δ = −43.1 ppm (51%), −50.7 ppm (32%), and −59.0 ppm (17%) corresponding to the T_0, T_1, and T_2 branches (see Figure 1). The observation of T_1 and T_2 branches is due to fact that moisture exposure during the sample preparation was not specifically avoided and the material had already undergone partially self-

Scheme 1. (A) Synthetic Route of DTMS-TPD: (a, b) Pd_2dba_3 (2 mmol %), DPPF (4 mmol %), NaOtertBu (2.8 equiv), Toluene, 15 h at 90 °C ((a) 86 and (b) 92% yield); (c) $POCl_3$, DMF, 0°C → 90°C, 15 h (60% yield); (d) $NaBH_4$, EtOH/Dichloromethane, 20 h, Room Temperature (96% yield); (e) NaH, Allyl Bromide, Dry THF, 0 °C → 5 h at 50 °C (68% yield); (f) Pt/C, $HSi(OMe)_3$, Toluene, 24 h at 90 °C (52% yield); (B) Formation of a Cross-Linked Siloxane Network of DTMS-TPD via Thermally Induced Condensation

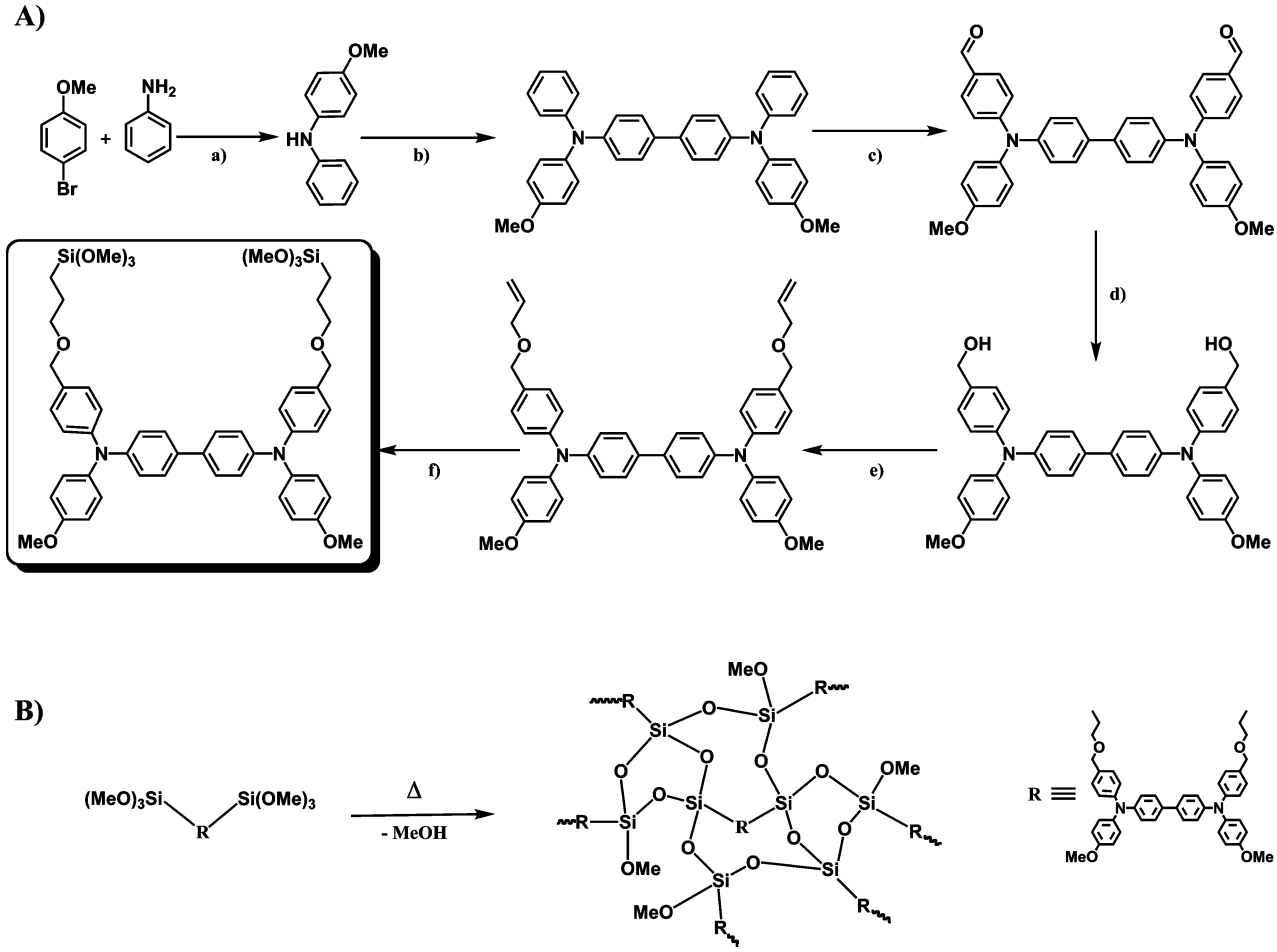

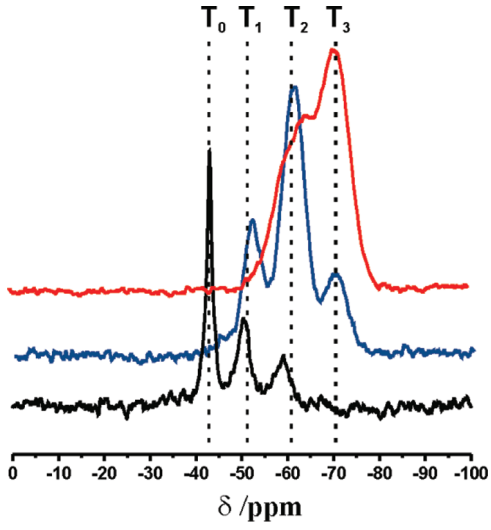

FIGURE 1. ^{29}Si-MAS NMR spectra of DTMS-TPD before thermal curing (black line), after exposure to air moisture for 18 h (blue line), and after thermal curing for 4 h at 160 °C (red line).

condensation before the actually measurement. But most of the siloxane was not condensed and the material was still completely soluble in toluene, dichlorobenzene, and tetrahydrofurane. Noteworthy, the partially condensed material actually showed better casting properties, e.g., no partially dewetting effects after spin-coating when compared to the freshly synthesized and noncondensed one were observed. It turned out that stirring all solutions of DTMS-TPD under an air atmosphere for 60 min before spin-coating was most beneficial for the spin-coating process.

Further exposure of the material to air moisture resulted in a further cross-linking of the bulk material, which was indicated by the most intensive T_2 signal in the ^{29}Si-MAS NMR spectrum. The T_0 signal completely disappeared and the sample was not completely soluble in THF anymore. After thermal treatment for 4 h at 160 °C, the ^{29}Si-MAS NMR spectrum showed only the T_2 and the T_3 signals, which indicated the formation of a highly cross-linked siloxane network showing good solvent resistance against tetahydrofurane and toluene. The reason for the minor amount of the remaining double condensed siloxane units indicated by the T_2 is probably due to steric hindrance of the remaining methoxy group in the rigid siloxane network and could not be further converted even after longer thermal treatment.

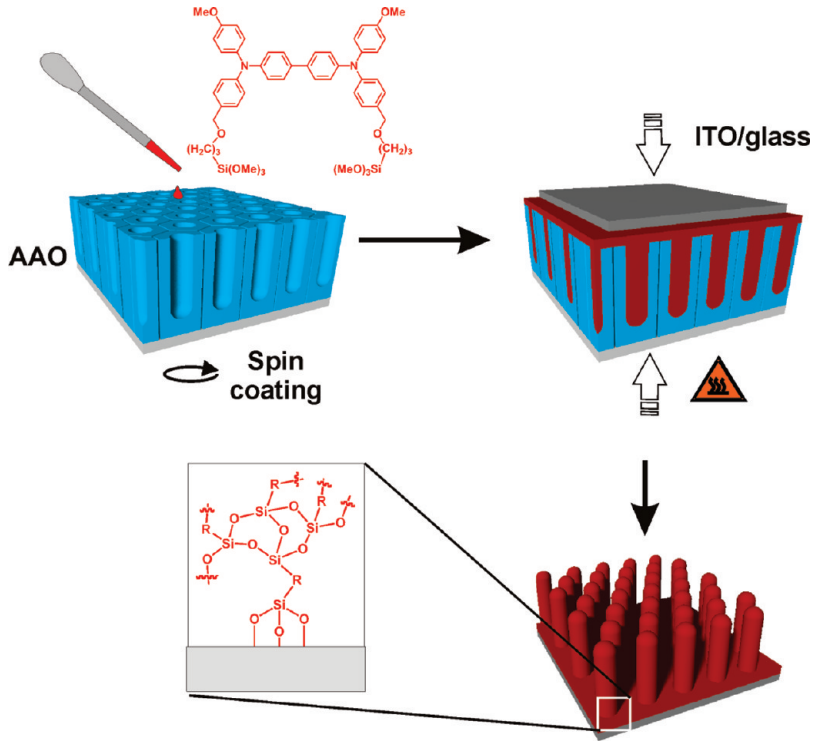

FIGURE 2. Schematic diagram of the template-assisted fabrication of cross-linked free-standing nanorod arrays.

Next, spin-coated and thermally cured films of DTMS-TPD on quartz with a film thickness of 100−150 nm were washed thoroughly with toluene, which is good solvent for the noncross-linked TPD monomer, and the UV/vis spectra of the thin films before and after washing were measured to estimate the amount of noncross-linked monomer/polymer after the thermal treatment process. After rinsing with toluene the absorption of the cured film showed only a slight decrease of less than 5%, which indicates a sufficient resistance against organic solvents as well as a satisfactory cross-linking reaction (see the Supporting Information, Figure S3).

The electrochemical properties of DTMS-TPD thin films were investigated by cyclic voltammetry (CV). As such, the CV curves of both the noncross-linked and the cross-linked films on ITO/glass were measured. Both showed the characteristic two oxidative peaks of the TPD moiety (see Figure 4). The cross-linking did not result in a shift of the redox potentials. Furthermore, the oxidation and reduction current, which is detected at the ITO electrode, indicated that the charge transport through the polymer film was not inhibited by the formation of the siloxane network. The highest occupied molecular orbital (HOMO) energy level was determined from the first oxidation peak to be −5.03 eV by using ferrocene/ferrocene$^+$ as a standard (E = −4.8 eV). Because of the two electron-rich methoxy substituents, the HOMO of DTMS-TPD exhibits a higher value and thus a smaller band gap to the work function of ITO (E = −4.7 eV) compared to other reported alkyl substituted TPD derivates ($E_{Homo} \approx -5.3$ eV) (40) was calculated. This shows promise for an enhanced hole injection efficiency from ITO to DTMS-TPD. The lowest unoccupied molecular orbital (LUMO) was estimated to be E = −2.27 eV, which was determined from the difference of the HOMO value and the optical band gap value of 2.76 eV, obtained from the lower energy onset of the absorption spectrum.

Template-Assisted Patterning. Well-ordered nanoporous AAO templates were used for the templating process of the TPD derivative. The AAO templates were fabricated in a two step anodization process as published recently (38). Detailed experimental information about the fabrication of the templates is given in the Supporting Information. The dimensional parameters, such as the interpore distance, length, and diameter of the pores could be varied and tailored to particular needs for the patterning by controlling the experimental parameters during the anodization process and by using an optional post pore widening process. To fulfill the morphological demands for the potential application in organic photovoltaics, only templates with a pore length in the range of 100−200 nm were used (see the Supporting Information, Figure S1).

The stepwise templating procedure is schematically illustrated in Figure 2. Because the thin AAO template is very fragile and can not be handled itself, the aluminum foil, which remains on the backside of the AAO after the anodization, was not directly removed and was used to mechanically stabilize the porous aluminum oxide during the patterning process. The pores of the AAO membrane were filled by wetting the topside of the membrane with the DTMS-TPD solution, followed by a subsequent imprinting step. The wetting via spin-coating of a diluted solution on top of the template resulted in a homogeneous coating and allowed to control the thickness of the DTMS-TPD layer on top of the template. Afterward, the coated template was imprinted on a conductive substrate, i.e.,ITO/glass or Pt-coated silicon. For

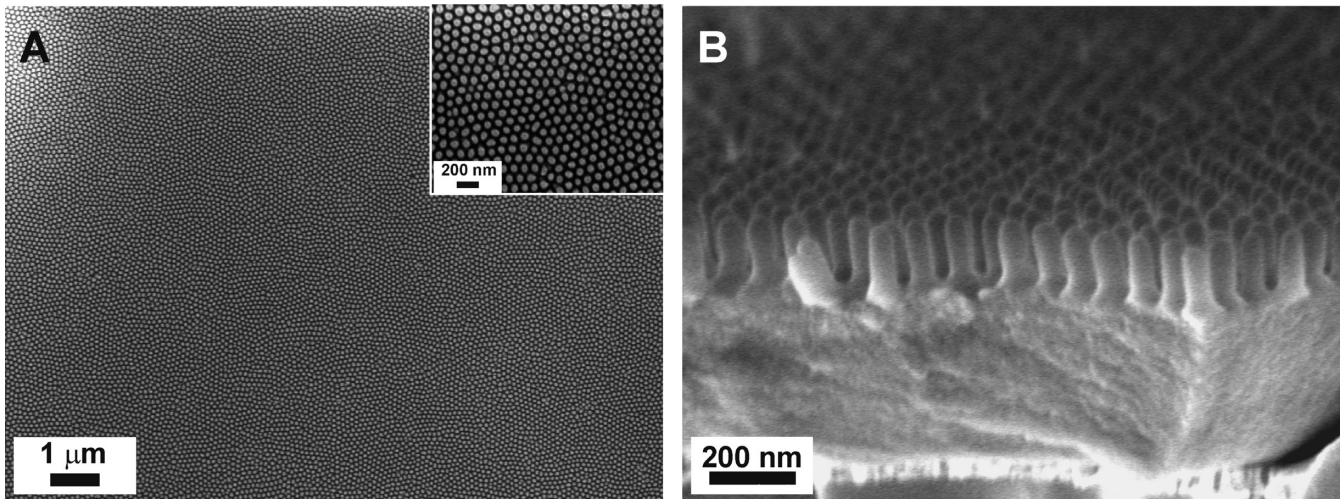

FIGURE 3. SEM images of free-standing cross-linked DTMS-TPD nanorod arrays with a length and diameter of 165 ± 5 nm and 64 ± 2 nm respectively. (A) Low-magnification top view of nanorod arrays on ITO/glass (inset, higher magnified image; scale bar, 200 nm); (B) cross-section of nanorod arrays on Pt-coated silicon substrate.

this purpose, the coated template was first pressed onto the substrate at 50 °C. Applied vacuum and the use of a PDMS layer between the sample and the pressing plates assured the removal of air inclusions and guaranteed a homogeneous imprinting pressure all over the sample. To increase the adhesion between the substrate and the TPD layer, the surface of the substrates was hydroxylated by a short O_2-plasma treatment prior the imprinting process. As a result, the trimethoxysilane groups could react with the hydroxy groups and covalently bind to the surface. After imprinting at 50 °C, the DTMS-TPD was thermally cured in vacuo at 160 °C for 3 h. Then, the aluminum layer was removed by treatment with a diluted $CuCl_2$ solution. Because of the instability of the cross-linking siloxane units against strong bases, the AAO template itself could not be removed by the commonly used treatment with aqueous KOH. Instead, the template was selectively removed by treatment with diluted phosphoric acid.

In explorative experiments, we have found that nanorods based on cross-linked DTMS-TPD with a length below 300 nm and an aspect ratio up to 5 exhibit a sufficient stiffness to prevent ground collapse after removal of the AAO scaffold. However, the nanorods tend to aggregate and form bundles after conventional drying. The capillary force upon drying is considered to be one of the main causes of aggregation (46–50). By applying a freeze-drying technique, following a procedure recently published (38), these capillary forces and consequently the formation of nanorod bundles were prevented and aggregation-free arrays were obtained.

Because the cured DTMS-TPD is covalently attached to the substrate, delamination effects, which were observed for different other cross-linkable materials without siloxane units, were drastically decreased and large macroscopic arrays of perfectly free-standing nanorods, which were all vertically aligned, had successfully been prepared by our method. For example, Figure 3 shows a top-view and cross-sectional SEM image of an aggregation-free array of DTMS-TPD nanorods on ITO/glass (Figure 3A) and Pt-coated silicon (Figure 3B). The lengths of the rods (170 nm) are in the appropriate range for photovoltaic application and the arrays provide a large surface that would allow the creation of a large well-ordered donor/acceptor interface.

To show that the thermal curing conditions are sufficient for a complete cross-linking and that the aqueous etching steps of the template do not affect the solvent resistance of the patterned DTMS-TPD, the UV/vis absorption of a patterned DTMS-TPD layer on a quartz substrate was measured before and after rinsing the substrate with toluene (see Figure 4A). In agreement with the results for the spin coated DTMS-TPD films the absorption spectra only showed a slight decrease in the absorption (<4%) after rinsing, which indicated a very good solvent resistance of the nanorod arrays even after the patterning procedure and the etching of the template under acidic conditions. Cyclovoltammetric measurements of the patterned film on ITO/glass showed no significant change of the electrochemical properties compared to the spin-coated and non cross-linked thin films (see Figure 4B). The CV curve still showed a reversible shape and the detectable oxidation and reduction current indicated a sufficient charge transport to the electrode.

The above-described results elucidate the macroscopic characteristics of the entire sample. However, for the application of such structures the homogeneity on a microscopic scale is of major interest. To investigate the properties of individual nanorods, we performed conductive scanning force microscopy (C-SFM). Here, an electrically conductive tip is scanned in contact mode over a surface at a constant normal force and bias voltage. Simultaneously to the topography, variations in the current through the tip are recorded. However, tip sample interactions and lateral forces. This can lead to bending and the complete destruction of fragile structures. The latter effect can be avoided by performing the C-SFM study in on a sample with stabilized nanorods. A stabilization can be achieved by only removing the supporting template on the topside (51, 52). Thus owing to the fragility of free standing polymer nanorod, only a few C-SFM studies were reported on organic free-standing nanorod arrays. Recently, Lee et al. reported on local conductivity

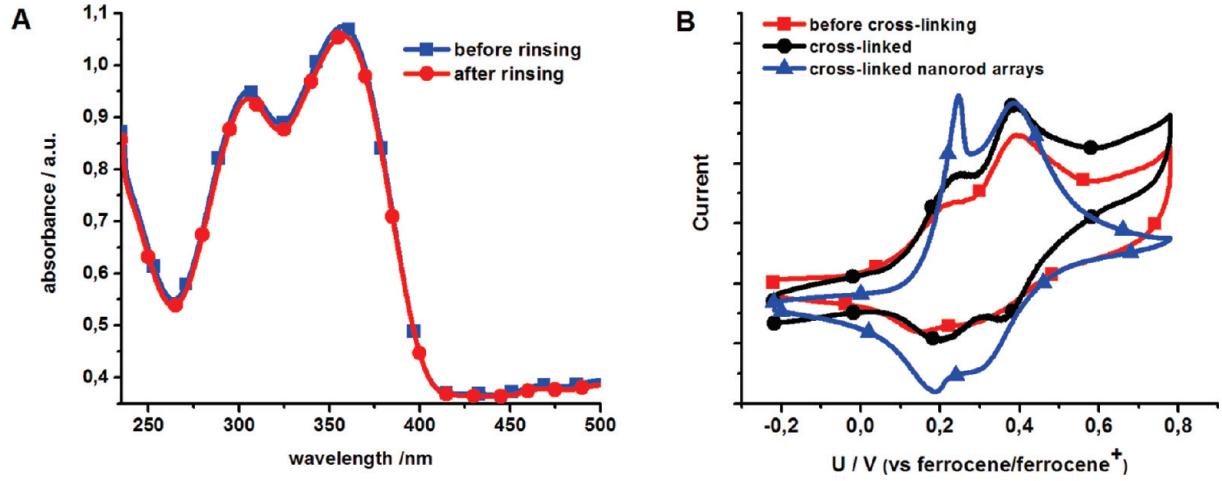

FIGURE 4. (A) Absorption spectra of an AAO-templated DTMS-TPD film on quartz (cured at 160 °C for 4 h) before (red line) and after rinsing (blue line) by toluene. (B) Cyclic voltammogram of a noncured (red line), cured (160 °C, 4 h) and cured AAO-templated (blue line) DTMS-TPD film on an ITO/glass substrate in a solution of n-Bu_4NPF_6 in acetonitrile (0.1 mol L^{-1}) at a scan rate of 0.1 V s^{-1}. The second scans are illustrated, respectively.

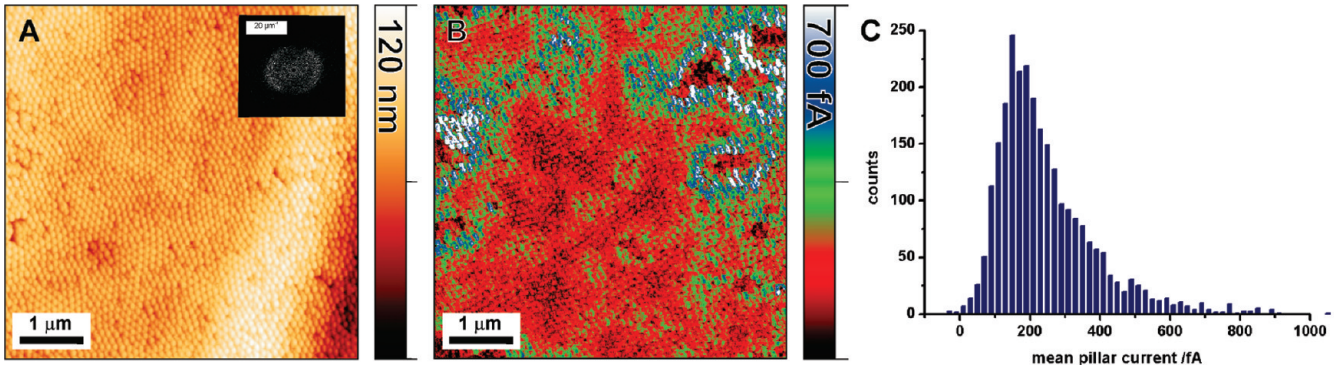

FIGURE 5. (A) Topography of a thermally cured DTMS-TPD nanorod array on a Si/Pt substrate. The inset shows a FFT analysis of the image (scale bar: 20 μm^{-1}). The halo at ~11 μm^{-1} corresponds to a mean nanorod distance of 90 nm. (B) Electrical current at V_{bias} = 12 V. (C) Histogram of the mean pillar currents of the 2660 nanorods visualized in (A) and (B).

measurements (without simultaneous topography mapping) of polyprrole nanopillars (32). Wang and co-worker presented C-SFM studies on the charge-carrier generation in illuminated low-aspect-ratio core/shell nanorods composed of polythiophene/fullerene (53).

Here, we avoid the destruction of individual nanorods by using a recently introduced C-SFM technique named scanning conductive torsion mode microscopy (SCTMM) (54). Because SCTMM is a noncontact mode, tip sample interactions and lateral forces are minimized. For this study, nanorod arrays were fabricated on Pt-coated Si wafers in order to minimize the surface roughness on the electrode. In the topographic image (Figure 5A), the well-aligned nanorod array could be clearly resolved with an average nanorod distance of 100 nm in consistence with the SEM studies (see Figure 3A). Because of its geometry, the tip could not completely penetrate into the voids between the rods and therefore the image showed a depth between the rods of only 30−40 nm. In the simultaneously recorded current map (Figure 5B) individual structures of the same average size and distance were observed. Each of these structures can be associated with the top part of an individual nanorod. By marking the positions of the 2660 nanorods in the topography image in Figure 5A and transferring them as a mask to the current map, the average current through each nanorod can be determined. Taking the average currents from all nanorods that were measured in one image, a current distribution was obtained (Figure 5C). From this histogram we find that more than 98% of the nanorods carry a current higher than 50 fA, i.e., higher than the noise level of the current measurement. The observation that almost every nanorod can conduct an electrical current of 250 ± 140 fA on average demonstrates that the electrical contact to the substrate is uniform and that there are no larger areas without contact to the substrate. Topographic features, such as the ridge in the lower right corner of Figure 5 A, do not have an observable influence on the electrical conductance of the sample. Moreover, we found that height differences between adjacent nanorods which would indicate differences in the nanorod length cannot be correlated with the current variations. Thus, the origin of the fluctuations is assigned to intrinsic conductivity variations in the rod material. Such fluctuations might be caused by variations in the alignment of the TPD moieties in the siloxane network.

CONCLUSION

The results shown in this contribution demonstrate that the AAO template-based fabrication of macroscopic arrays

of well-ordered nanorods, which are vertically aligned and noncollapsed on conductive substrates and composed of a hole-conducting trimethoxysilane-substituted tetraphenylbenzydine derivative (DTMS-TPD), is very feasible. Nonaggregated nanorod arrays were replicated on the substrate by solution wetting and imprinting of the AAO template. The DTMS-TPD could thermally be cross-linked at 160 °C and showed high resistance against organic solvents in bulk, within thin films and also within nanorod arrays. Because of covalent attachment onto the substrate during the thermal curing, the films also exhibited a good mechanical adhesion to the substrate. The local electrical properties were investigated with conductive scanning torsion mode microscopy (SCTMM). It revealed a good and homogeneous electrical connection of the DTMS-TPD nanostructures to the substrate. Furthermore, 98% of the nanorods were carrying a current significantly above the noise level. Finally, samples were investigated by cyclovoltammetry, which indicated good hole-conducting behavior of the DTMS-TPD. Therefore, these nanorod arrays are highly interesting for the fabrication of multilayered device architectures to be used in organic photovoltaics.

Acknowledgment. The authors thank B. Mathiasch for their help of solid-state NMR measurements and H.-J. Butt and U. Rietzler for discussion and support. The Electron Microscopy at the Max-Planck Institute for Polymer Research in Mainz, in particular G. Glasser, is acknowledged for access to SEM measurements. This research was supported by the DFG (IRTG 1404) and by the WCU (World Class University) program through the National Research Foundation of Korea funded by the Ministry of Education, Science and Technology (R31-10013)

Supporting Information Available: Fabrication and SEM micrographs of AAO templates, TGA data, and UV/vis diagrams of spin-coated cross-linked DTMS-TPD before and after rinsing with toluene (PDF). This material is available free of charge via the Internet at http://pubs.acs.org.

REFERENCES AND NOTES

(1) Menard, E.; Meitl, M.; Sun, Y.; Park, J.; Shir, D.; Nam, Y.; Jeon, S.; Rogers, J. *Chem. Rev.* **2007**, *107*, 1117–1160.
(2) Hohnholz, D.; Okuzaki, H.; MacDiarmid, A. *Adv. Funct. Mater.* **2005**, *15*, 51–56.
(3) Wallraff, G.; Hinsberg, W. *Chem. Rev.* **1999**, *99*, 1801–1822.
(4) Gather, M. C.; Köhnen, A.; Falcou, A.; Becker, H.; Meerholz, K. *Adv. Funct. Mater.* **2007**, *17*, 191–200.
(5) de Gans, B.-J.; Duineveld, P. C.; Schubert, U. S. *Adv. Mater.* **2004**, *16*, 203–213.
(6) Sirringhaus, H.; Kawase, T.; Friend, R.; Shimoda, T.; Inbasekaran, M.; Wu, W.; Woo, E. *Science* **2000**, *290*, 2123–2126.
(7) Xia, Y.; Yang, P.; Sun, Y.; Wu, Y.; Mayers, B.; Gates, B.; Yin, Y.; Kim, F.; Yan, H. *Adv. Mater.* **2003**, *15*, 353–389.
(8) Lee, W.; Scholz, R.; Nielsch, K.; Gösele, U. *Angew. Chem., Int. Ed.* **2005**, *44.*, 6050–6054.
(9) Choi, J.; Sauer, G.; Nielsch, K.; Wehrspohn, R.; Gösele, U. *Chem. Mater.* **2003**, *15*, 776–779.
(10) Hu, W.; Gong, D.; Chen, Z.; Yuan, L.; Saito, K.; Grimes, C.; Kichambare, P. *Appl. Phys. Lett.* **2001**, *79*, 3083–3085.
(11) Haberkorn, N.; Lechmann, M. C.; Sohn, B. H.; Char, K.; Gutmann, J. S.; Theato, P. *Macromol. Rapid Commun.* **2009**, *30*, 1146–1166.
(12) Coakley, K.; McGehee, M. *Chem. Mater.* **2004**, *16*, 4533–4542.
(13) Gunes, S.; Neugebauer, H.; Sariciftci, N. *Chem. Rev.* **2007**, *107*, 1324–1338.
(14) Yang, X.; Loos, J. *Macromolecules* **2007**, *40*, 1353–1362.
(15) Masuda, H.; Fukuda, K. *Science* **1995**, *268*, 1466–1468.
(16) Li, A.; Muller, F.; Birner, A.; Nielsch, K.; Gösele, U. *J. Appl. Phys.* **1998**, *84*, 6023–6026.
(17) Nielsch, K.; Choi, J.; Schwirn, K.; Wehrspohn, R.; Gösele, U. *Nano Lett.* **2002**, *2*, 677–680.
(18) Masuda, H.; Yamada, H.; Satoh, M.; Asoh, H.; Nakao, M.; Tamamura, T. *Appl. Phys. Lett.* **1997**, *71*, 2770–2772.
(19) Li, F.; Zhang, L.; Metzger, R. *Chem. Mater.* **1998**, *10*, 2470–2480.
(20) Park, S.; Wang, J.-Y.; Kim, B.; Xu, J.; Russell, T. *ACS Nano* **2008**, *2*, 766–772.
(21) Thurn-Albrecht, T.; Schotter, J.; Kastle, G.; Emley, N.; Shibauchi, T.; Krusin-Elbaum, L.; Guarini, K.; Black, C.; Tuominen, M.; Russell, T. *Science* **2000**, *290*, 2126–2129.
(22) Thurn-Albrecht, T.; Steiner, R.; DeRouchey, J.; Stafford, C.; Huang, E.; Bal, M.; Tuominen, M.; Hawker, C.; Russell, T. *Adv. Mater.* **2000**, *12*, 787–791.
(23) Kim, T.-Y.; Jeong, S.-H.; Korean, J. *Chem. Eng.* **2008**, *25*, 609–611.
(24) Park, S.; Lee, D.; Xu, J.; Kim, B.; Hong, S.; Jeong, U.; Xu, T.; Russell, T. *Science* **2009**, *323*, 1030–1033.
(25) Liang, Y.; Zhen, C.; Zou, D.; Xu, D. *J. Am. Chem. Soc.* **2004**, *126*, 16338–16339.
(26) Demoustier-Champagne, S.; Stavaux, P. *Chem. Mater.* **1999**, *11*, 829–834.
(27) Yang, S.; Chen, K.; Yang, Y. *Synth. Met.* **2005**, *152*, 65–68.
(28) Xiao, R.; Cho, S.; Liu, R.; Lee, S. *J. Am. Chem. Soc.* **2007**, *129*, 4483–4489.
(29) Steinhart, M.; Shimazu, T.; Shimazu, T.; Steinhart, M. *Adv. Polym. Sci.* **2008**, *220*, 123–187.
(30) Steinhart, M.; Wendorff, J.; Greiner, A.; Wehrspohn, R.; Nielsch, K.; Schilling, J.; Choi, J.; Gösele, U. *Science* **2002**, *296*, 1997.
(31) Steinhart, M.; Wendorff, H. J.; Wehrspohn, Ralf *Chem. Phys. Chem.* **2003**, *4*, 1171–1176.
(32) Lee, J. I.; Cho, S. H.; Park, S.-M.; Kim, J. K.; Kim, J. K.; Yu, J.-W.; Kim, Y. C.; Russell, T. P. *Nano Lett.* **2008**, *8*, 2315–2320.
(33) Berdichevsky, Y.; Lo, Y. *Adv. Mater.* **2006**, *18*, 122–125.
(34) Park, D.; Kim, B.; Jang, M.; Bae, K.; Joo, J. *Appl. Phys. Lett.* **2005**, *86*, 113116.
(35) Bai, R.; Ouyang, M.; Zhou, R.-J.; Shi, M.-M.; Wang, M.; Chen, H.-Z. *Nanotechnology* **2008**, *19*, 055604.
(36) Li, X.; Tian, S.; Ping, Y.; Kim, D.; Knoll, W. *Langmuir* **2005**, *21*, 9393–9397.
(37) Goh, C.; Coakley, K.; McGehee, M. *Nano Lett.* **2005**, *5*, 1545.
(38) Haberkorn, N.; Gutmann, J. S.; Theato, P. *ACS Nano* **2009**, *3*, 1415–1422.
(39) Cui, J.; Huang, Q.; Wang, Q.; Marks, T. *Langmuir* **2001**, *17*, 2051–2054.
(40) Li, J.; Marks, T. J. *Chem. Mater.* **2008**, *20*, 4873–4882.
(41) Yan, H.; Huang, Q.; Cui, J.; Veinot, J.; Kern, M.; Marks, T. *Adv. Mater.* **2003**, *15*, 835.
(42) Yan, H.; Lee, P.; Armstrong, N.; Graham, A.; Evmenenko, G.; Dutta, P.; Marks, T. *J. Am. Chem. Soc.* **2005**, *127*, 3172–3183.
(43) Veinot, J.; Marks, T. *Acc. Chem. Res.* **2005**, *38*, 632–643.
(44) Kessler, D.; Theato, P. *Macromolecules* **2008**, *41*, 5237–5244.
(45) Sakamoto, S.; Shimojima, A.; Miyasaka, K.; Ruan, J.; Terasaki, O.; Kuroda, K. *J. Am. Chem. Soc.* **2009**, *131*, 9634–9635.
(46) Fan, J.; Dyer, D.; Zhang, G.; Zhao, Y. *Nano Lett.* **2004**, *4*, 2133–2138.
(47) Chandra, D.; Taylor, J. A.; Yang, S. *Soft Matter* **2008**, *4*, 979–984.
(48) Chandra, D.; Yang, S.; Soshinsky, A. A.; Gambogi, R. J. *ACS Appl. Mater. Interfaces* **2009**, *1*, 1698–1704.
(49) Chen, G.; Soper, S.; McCarley, R. *Langmuir* **2007**, *23*, 11777–11781.
(50) Tanaka, T.; Morigami, M.; Oizumi, H.; Ogawa, T. *Jpn. J. Appl. Phys.* **1993**, *32*, 5813–5814.
(51) Wang, K.; Birjukovs, P.; Erts, D.; Phelan, R.; Morris, M. A.; Zhou, H.; Holmes, J. D. *J. Mater. Chem.* **2009**, *19*, 1331–1338.
(52) Erts, D.; Polyakov, B.; Dalyt, B.; Morris, M.; Ellingboe, S.; Boland, J.; Holmes, J. *J. Phys. Chem. B* **2006**, *110*, 820–826.
(53) Wang, H.-S.; Lin, L.-H.; Chen, S.-Y.; Wang, Y.-L.; Wei, K.-H. *Nanotechnology* **2009**, *20*, 075201.
(54) Berger, R.; Butt, H.-J.; Retschke, M. B.; Weber, S. A. L. *Macromol. Rapid Commun.* **2009**, *30*, 1167–1178.

AM100085T